Absorption spectrum of Ca atoms attached to ^{4}He nanodroplets

Alberto Hernando, Manuel Barranco, Ricardo Mayol, and Martí Pi

Departament ECM, Facultat de Física, and IN^2 *UB, Universitat de Barcelona, Diagonal 647, 08028 Barcelona, Spain*

Marek Krośnicki

Institute of Theoretical Physics and Astrophysics, University of Gdansk, ul Wita Stwosza 57, PL80 Gdansk, Poland

Within density functional theory, we have obtained the structure of ^{4}He droplets doped with neutral calcium atoms. These results have been used, in conjunction with newly determined *ab initio* $^1\Sigma$ and $^1\Pi$ Ca-He pair potentials, to address the $4s4p\ ^1P_1 \leftarrow 4s^2\ ^1S_0$ transition of the attached Ca atom, finding a fairly good agreement with absorption experimental data. We have studied the drop structure as a function of the position of the Ca atom with respect to the center of mass of the helium moiety. The interplay between the density oscillations arising from the helium intrinsic structure and the density oscillations produced by the impurity in its neighborhood plays a role in the determination of the equilibrium state, and hence in the solvation properties of alkaline earth atoms. In a case of study, the thermal motion of the impurity within the drop surface region has been analyzed in a semiquantitative way. We have found that, although the atomic shift shows a sizable dependence on the impurity location, the thermal effect is statistically small, contributing by about 10% to the line broadening. The structure of vortices attached to the calcium atom has been also addressed, and its effect on the calcium absorption spectrum discussed. At variance with previous theoretical predictions, we conclude that spectroscopic experiments on Ca atoms attached to ^{4}He drops will be likely unable to detect the presence of quantized vortices in helium nanodrops.

I. INTRODUCTION

Optical investigations of atomic impurities in superfluid helium nanodroplets have drawn considerable attention in recent years.[1,2] In particular, the shifts of the electronic transition lines with respect to the gas-phase transition lines (atomic shifts) are a very useful observable to determine the location of the foreign atom attached to the drop. Alkaline earth atoms appear to play a unique role in this context. While, e.g., all alkali atoms reside in surface "dimple" states, and more attractive impurities such as all noble gas atoms reside in the bulk of drops made of either isotope,[3] the absorption spectra of heavy alkaline earth atoms attached to ^{4}He drops clearly support an outside location of Ca, Sr, and Ba,[4,5] whereas for the lighter Mg atom the experimental evidence is that it resides in the bulk of the ^{4}He droplets.[6,7]

We have recently presented density functional theory (DFT) results for the structure and energetics of large ^{3}He and ^{4}He doped nanodroplets, showing that alkaline earth atoms from Mg to Ba go to the bulk of ^{3}He drops, whereas Ca, Sr, and Ba reside in a dimple at the surface of ^{4}He drops, and Mg is in their interior.[8] This is in agreement with the analysis of available experimental data, although the case of Mg has been questioned very recently.[9] Moreover, according to the magnitude of the observed shifts, the dimple for alkaline earth atoms was thought to be more pronounced than for alkali atoms, indicating that the former reside deeper inside the drop than the latter. This has been also confirmed by the calculations. In addition, the $5s5p \leftarrow 5s^2$ experimental transition of Sr atoms attached to helium nanodroplets of either isotope has shown that strontium is solvated inside ^{3}He nanodroplets, also in agreement with the calculations.[8]

Calcium atoms are barely stable on the surface of the drop, and the difference between the energy of the surface dimple state and that of the solvated state in the bulk of the drop is rather small and depends very sensitively on the Ca-He interatomic potential.[10] The aim of this work is to obtain the atomic shifts for Ca attached to large ^{4}He drops, and to compare them with the experimental data. To this end, we have improved our DFT approach,[8] treating the atomic impurity as a quantal particle instead of as an external field. Laser induced fluorescence (LIF) experiments for Ca atoms in liquid ^{3}He and ^{4}He have been reported[11] and analyzed within a vibrating bubble model, which involves the formation of a bubble around the impurity, using Ca-He pair potentials based on pseudopotential self-consistent field/configuration interaction (SCF/CI) calculations.[12]

This work is organized as follows. In Sec. II we discuss the Ca-He interaction potentials we have used. In Sec. III we briefly present our density functional approach, as well as some illustrative results for the structure of Ca@^{4}He$_N$ drops. The method we have employed to obtain the atomic shifts is discussed in Sec. IV. In Sec. V we present the results obtained for calcium, discuss how thermal motion may affect the line shapes, and investigate how the presence of a quantized vortex line may change the Ca absorption spectrum. Finally, a summary is presented in Sec. VI.

II. CALCIUM-HELIUM INTERACTION POTENTIALS

Figure 1 shows the $X\ ^1\Sigma$ Ca-He adiabatic potential obtained by different authors.[13–16] This potential determines the dimple structure described in the next section. It can be seen that apart from the unpublished potential by Meyer, the others are quite similar. As in our previous work,[8] we shall use the one obtained in Ref. 15. This will allow us to ascertain the effect of treating Ca as a quantal particle. Since the $X\ ^1\Sigma$ potential seems to be fairly well determined, we have turned
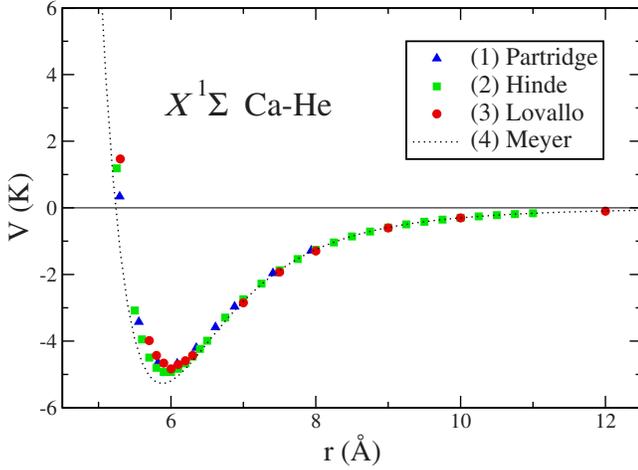
FIG. 1. (Color online) Some recent $X\,^1\Sigma$ Ca-He pair potentials: (1) Ref. 13, (2) Ref. 14, (3) Ref. 15, and (4) Ref. 16.

FIG. 2. (Color online) Excited Ca-He pair potentials used in this work.

our attention to the excited adiabatic potentials.

In a previous work[17] the excited state potentials were calculated in a valence *ab initio* scheme. The core electrons of calcium and helium were replaced by scalar-relativistic energy-consistent pseudopotentials, and the energy curves were calculated on the complete-active-space multiconfiguration self-consistent field (CASSCF)[18,19]/complete-active-space multireference second order perturbation level of theory.

In this work we have performed fully *ab initio* calculations and have only focused on singlet states. The calculations for excited states have been done at the CASSCF/internally contracted multireference configuration interaction (ICMRCI)[20,21] level of theory. In the calculations we have used correlation consistent polarized valence five zeta basis sets. For the calcium atom we have used the $(26s,18p,8d,3f,2g,1h)/[8s,7p,5d,3f,2g,1h]$ basis set developed by Koput and Peterson,[22] and for the helium atom we have used the $(8s,4p,3d,2f,1g)/[5s,4p,3d,2f,1g]$ basis set developed by Woon and Dunning.[23]

The calculations were performed within the MOLPRO suite of *ab initio* programs.[24] The molecular orbitals used for the excited state calculations were optimized in the state averaged CASSCF method for all singlet states correlating to $(4s^2)\,^1S$, $(4s3d)\,^1D$, and $(4s4p)\,^1P$ atomic asymptotes. The active space was formed by distributing the two valence electrons of the Ca atom into $4s3d4p$ valence orbitals. The $1s2s2p3s3p$ orbitals of calcium and $1s$ orbital of helium were kept doubly occupied in all configuration state functions, but they were optimized in the CASSCF calculations. The resulting wave functions were used as references in the following ICMRCI calculations. At the ICMRCI level, the $1s2s2p3s3p$ orbitals of calcium and $1s$ orbital of helium were kept as doubly occupied in all reference configuration state functions, but these orbitals were correlated through single and double excitations. The $4s$, $4p$, and $3d$ calcium orbitals had not restricted occupation patterns. We show in Fig. 2 the excited adiabatic potentials; to have better insight into the potential minima of the $^1\Sigma$ and $^1\Pi$ potentials, they have been plotted correlating to the $(4p)\,^1P$ Ca term.
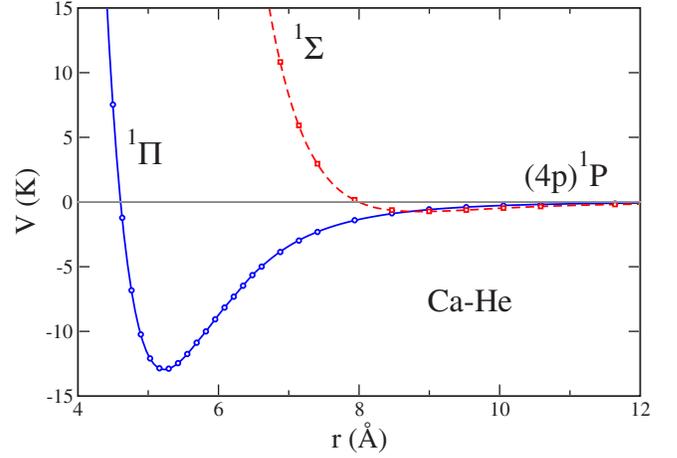
III. DENSITY FUNCTIONAL THEORY DESCRIPTION OF HELIUM NANODROPLETS

In recent years, static and time-dependent density functional methods[25–27] have become increasingly popular to study inhomogeneous liquid helium systems because they provide an excellent compromise between accuracy and computational effort, allowing us to address problems inaccessible to more fundamental approaches, see, e.g., Ref. 3 for a recent review. Obviously, DFT cannot take into account the atomic, discrete nature of these systems, but can address inhomogeneous helium systems at the nanoscale[28] and take into account the anisotropic deformations induced by some dopants in helium drops. Both properties are essential to properly describe these systems.

Our starting point is the Orsay-Trento density functional,[25] together with the Ca-He adiabatic potential $X\,^1\Sigma$ of Ref. 15, here denoted as $V_{\text{Ca-He}}$. This allows us to write the energy of the Ca-drop system as a functional of the Ca wave function $\Phi(\mathbf{r})$ and the ^{4}He "order parameter" $\Psi(\mathbf{r})$ as follows:

$$
\begin{aligned}
E[\Psi,\Phi] = &\frac{\hbar^2}{2m_{\text{He}}}\int d^3\mathbf{r}\,|\nabla\Psi(\mathbf{r})|^2 + \int d^3\mathbf{r}\,\mathcal{E}(\rho) \\
&+ \frac{\hbar^2}{2m_{\text{Ca}}}\int d^3\mathbf{r}\,|\nabla\Phi(\mathbf{r})|^2 \\
&+ \int\int d^3\mathbf{r}\,d^3\mathbf{r}'\,|\Phi(\mathbf{r})|^2 V_{\text{Ca-He}}(|\mathbf{r}-\mathbf{r}'|)\rho(\mathbf{r}').
\end{aligned}
$$

$$(1)$$

The order parameter is defined as $\Psi(\mathbf{r})=\sqrt{\rho(\mathbf{r})}\exp[\iota S(\mathbf{r})]$, where $\rho(\mathbf{r})$ is the particle density and $\mathbf{v}(\mathbf{r})=\hbar\nabla S(\mathbf{r})/m_4$ is the velocity field of the superfluid. In Eq. (1), $\mathcal{E}(\rho)$ is the ^{4}He "potential energy density."[25] In the absence of vortex lines, we set S to zero and E becomes a functional of ρ and Φ. Otherwise, we have used the complex order parameter $\Psi(\mathbf{r})$ to describe the superfluid.

We have solved the Euler-Lagrange equations which result from the variations with respect to Ψ^* and Φ^* of the

energy $E[\Psi,\Phi]$ under the constrain of a given number of helium atoms in the drop, and a normalized Ca wave function, namely,

$$-\frac{\hbar^2}{2m_{He}}\Delta\Psi + \left\{\frac{\delta\mathcal{E}}{\delta\rho} + U_{He}\right\}\Psi = \mu\Psi \qquad (2)$$

$$-\frac{\hbar^2}{2m_{Ca}}\Delta\Phi + U_{Ca}\Phi = \varepsilon\Phi, \qquad (3)$$

where μ is the helium chemical potential and ε is the lowest eigenvalue of the Schrödinger equation obeyed by the Ca atom. The effective potentials U_{He} and U_{Ca} are defined as

$$U_{He}(\mathbf{r}) = \int d^3\mathbf{r}' |\Phi(\mathbf{r}')|^2 V_{Ca\text{-}He}(|\mathbf{r}-\mathbf{r}'|),$$

$$U_{Ca}(\mathbf{r}) = \int d^3\mathbf{r}' \rho(\mathbf{r}') V_{Ca\text{-}He}(|\mathbf{r}-\mathbf{r}'|). \qquad (4)$$

The coupled equations (2) and (3) have to be solved self-consistently, starting from an arbitrary but reasonable choice of the unknown functions Ψ and Φ. In spite of the axial symmetry of the problem, we have solved them in three-dimensional (3D) Cartesian coordinates. The main reason is that these coordinates allow us to use fast Fourier transformation techniques[29] to efficiently compute the convolution integrals entering the definition of $\mathcal{E}(\rho)$, i.e., the mean field helium potential and the coarse-grained density needed to compute the correlation term in the He density functional,[25] as well as the fields defined in Eq. (4).

The differential operators in Eqs. (1)–(3) have been discretized using 13-point formulas for the derivatives, and Eqs. (2) and (3) have been solved employing an imaginary time method;[30] some technical details of our procedure are given in Ref. 31. Typical calculations have been performed using a spatial mesh step of 0.5 Å. We have checked the stability of the solutions against reasonable changes in the step.

Equations (2) and (3) have been solved for several N values from 100 to 2000. They will allow us to study the atomic shift as a function of the cluster size. The equilibrium configurations of Ca@^{4}He$_{1000}$ and Ca@^{4}He$_{2000}$ will be shown later.

Figure 3 shows the energy of a Ca atom attached to a drop, defined as the energy difference

$$S_N(Ca) = E(Ca@^4He_N) - E(^4He_N). \qquad (5)$$

On the figure are shown also the results obtained treating calcium as an external field.[8] It can be seen that for large drops the energy of the calcium atom is about 10 K less negative due to its zero point motion. We want to stress again how barely stable is the calcium atom on the surface of ^{4}He$_N$ drops. For instance, we have found that the total energy of the equilibrium—dimple—configuration of Ca@^{4}He$_{1000}$ is ~ -5467.4 K, whereas it is ~ -5455.0 K when Ca is forced to be at the center of the drop. For Ca@^{4}He$_{500}$, the corresponding values are ~ -2525.2 and ~ -2511.1 K, respectively.
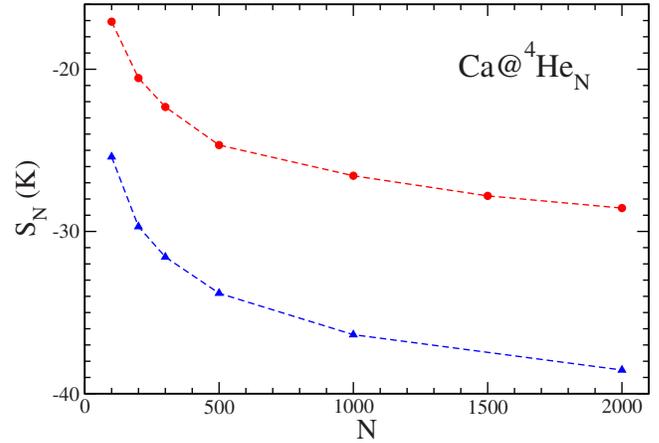

FIG. 3. (Color online) Energy (K) of a calcium atom as a function of the number of ^{4}He atoms in the droplet (dots). Results obtained treating calcium as an external field are also shown (triangles) (Ref. 8). The lines have been drawn to guide the eyes.

The dimple depth ξ, defined as the difference between the position of the dividing surface at $\rho = \rho_0/2$, where $\rho_0 = 0.0218$ Å^{-3} is the bulk liquid density, with and without impurity, respectively, is shown in Fig. 4. Due to the zero point motion that pushes the impurity toward lower helium densities, for large drops the dimple depth is about 0.8 Å smaller when the zero point motion is included than when it is not.[8] This change in the depth is large enough to produce observable effects in the calculated absorption spectrum, as discussed below.

It can be seen that the dimple depth curve $\xi(N)$ has some structure. This is not a numerical artifact, but a genuine effect due to the interplay between the Ca atom and the drop, whose density, even for pure drops, shows conspicuous oscillations all over the drop volume, extending up to the surface region irrespective of whether the drop is described within DFT or diffusion Monte Carlo methods.[3,25,32] The interplay of these oscillations with those arising from the presence of the impurity little affects the total energy of the sys-
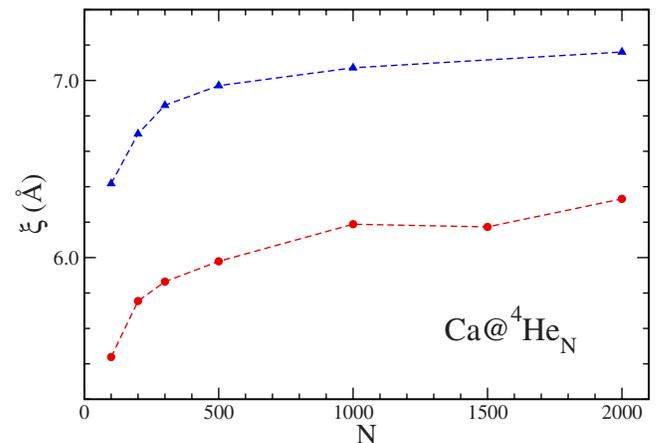

FIG. 4. (Color online) Calcium dimples (Å) as a function of the number of ^{4}He atoms in the droplet (dots). Results obtained treating calcium as an external field (Ref. 8) are also shown (triangles). The lines have been drawn to guide the eyes.
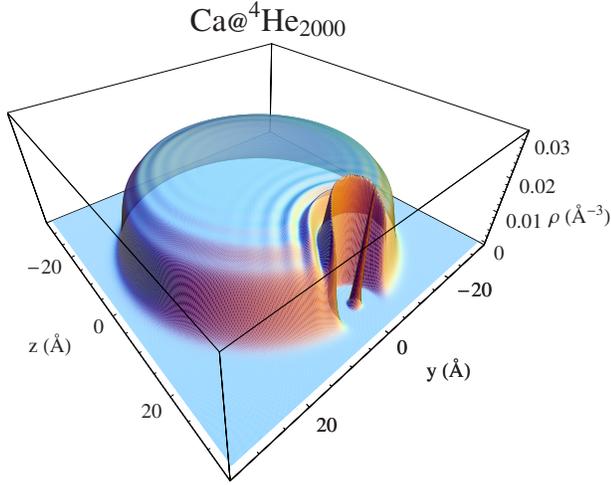
FIG. 5. (Color online) Helium density of the Ca@^{4}He$_{2000}$ drop on the $x=0$ plane. The probability density of the calcium atom is also shown, rescaled multiplying it by a ρ_0 factor for the sake of clarity.

tem and hence, the Ca energy, but yields some visible structure in the density distributions that shows up in related quantities, such as the dimple depth. To illustrate it, we show in Fig. 5 the density of the helium moiety of Ca@^{4}He$_{2000}$, where the interference pattern can be clearly seen.

Further insight can be gained studying, for a given drop, the energy of the Ca@^{4}He$_N$ complex as a function of the distance between the centers of mass of the impurity and of the helium moiety. This can be done adding an appropriate constraint to the total energy in Eq. (1), and solving the corresponding Euler-Lagrange equations. Specifically, we have minimized the expression

$$E + \frac{\lambda_C}{2}[\mathcal{Z} - \mathcal{Z}_0]^2, \qquad (6)$$

where $\mathcal{Z}$ is the average distance in the z direction between the impurity and the geometrical center of the helium moiety

$$\mathcal{Z} = \int d\mathbf{r}^3 z |\Phi(\mathbf{r})|^2 - \frac{1}{N}\int d\mathbf{r}^3 z \rho(\mathbf{r}), \qquad (7)$$

and λ_C is an arbitrary constant, large enough to guarantee that upon minimization, $\mathcal{Z}$ equals the desired $\mathcal{Z}_0$ value. We have also applied this method to Mg doped helium drops, and will present the details of the calculation elsewhere.[33]

We show in the bottom panel of Fig. 6 the total energy of the Ca@^{4}He$_{500}$ and Ca@^{4}He$_{1000}$ systems as a function of $\mathcal{Z}_0$. For the sake of comparison, the energies and $\mathcal{Z}_0$ distances are referred to their equilibrium values. The vertical lines roughly delimit the drop surface regions, conventionally defined as the radial distance between the points where the density equals $0.1\rho_0$ and $0.9\rho_0$ (see Fig. 10). The horizontal line has been drawn 0.4 K above the equilibrium energy, representing the accessible energy range due to the temperature of the helium drops.[34] Its intersection with the energy curves yields a qualitative measure of the dispersion of the impurity location due to thermal motion. The energy curve of
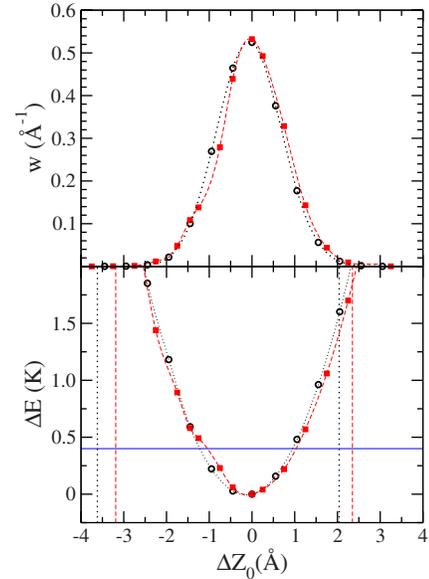

FIG. 6. (Color online) Bottom panel: Total energy (K) of Ca@^{4}He$_{500}$ (circles) and Ca@^{4}He$_{1000}$ (squares) as a function of $\mathcal{Z}_0$ (Å), both referred to their equilibrium values. The vertical lines delimit the drop surface regions, and the horizontal line has been drawn 0.4 K above the equilibrium energy. Top panel: Probability densities for the configurations displayed in the bottom panel. Circles correspond to Ca@^{4}He$_{500}$ and squares to Ca@^{4}He$_{1000}$. In both panels, dotted lines refer to the $N=500$ drop and dashed lines to the $N=1000$ drop; the lines (cubic splines) have been drawn to guide the eyes.

Ca@^{4}He$_{1000}$ displays some structure to the left of the minimum due to the mentioned interference pattern. This behavior has not been disclosed before, and appears in the course of "pushing" the impurity inside the droplet from its equilibrium position (a similar structure shows up for Ca@^{4}He$_{500}$, but at more negative $\Delta\mathcal{Z}_0$ values). While it affects rather little the equilibrium location of the Ca atom because of its clear surface location, and hence the atomic shift—see, however, the inset in Fig. 8, it plays a substantial role in the solvation of magnesium atoms in small helium drops.[33] We recall that this problem has recently drawn the attention of experimentalists and theoreticians as well.[6–9,35,36] How the position of the Ca atom affects the absorption spectrum throughout the change in the dimple structure will be discussed in Sec. V.

IV. EXCITATION SPECTRUM OF AN ATOMIC IMPURITY IN A ^{4}He DROP

Lax's method[37] offers a realistic way to study the absorption spectrum $I(\omega)$ of a foreign atom embedded in helium drops. It makes use of the Franck-Condon principle within a semiclassical approach, and it has been employed to study the absorption spectrum of several atomic dopants attached to fairly small ^{4}He drops.[35,38–40] The case of alkali atoms attached to large drops described within DFT has been also considered, see Refs. 41 and 42, and references therein. Lax's method is usually applied in conjunction with the

diatomics-in-molecules theory,[43] which means that the atom-drop complex is treated as a diatomic molecule, where the helium moiety plays a role of the other atom.

In the original formalism, to obtain $I(\omega)$ one has to carry out an average on the possible initial states of the system that may be thermally populated. Usually, this average is not needed for helium drops, as their temperature, about 0.4 K,[34] is much smaller than the vibrational excitation energies of the Ca atom in the mean field represented by the second term of Eq. (4).[44] However, thermal broadering due to the "wandering" of the dopant must be analyzed separately if it is in a dimple state, as this may have some influence on the line shape. Its effect on the absorption spectrum will be exemplified later for the $N=500$ case. Contrarily, when the impurity is very attractive and resides in the bulk of the drop, thermal motion plays no role, as the dopant hardly gets close enough to the drop surface to have some effect on the line shape. In this case, dynamical deformations of the cavity around the impurity may be relevant (Jahn-Teller effect). It cannot be discarded that, if some of these very attractive impurities have an angular momentum large enough,[45] they may get close to the drop surface, in which case thermal motion might have some influence on the absorption spectrum.

We review here the essentials of the method and the way we have implemented it. In particular, we present some of the expressions in Cartesian coordinates, better adapted to our approach. They are of course equivalent to the expressions in spherical coordinates that can be found in the literature—see, e.g., Ref. 39 and references therein.

A. Line shapes

The line shapes for electronic transitions from the ground state (gs) to the excited state (ex) in a condensed phase system can be written as

$$I(\omega) \propto \int dt e^{-i\omega t} \langle \Psi^{gs} | D_{ge}^\dagger e^{(it/\hbar)\mathcal{H}_{ex}} D_{ge} e^{-(it/\hbar)\mathcal{H}_{gs}} | \Psi^{gs} \rangle, \quad (8)$$

where D_{ge} is the matrix element of the electric dipole operator, $\mathcal{H}_{gs}$ and $\mathcal{H}_{ex}$ are the Hamiltonians which describe the ground and excited states of the system, respectively, and $|\Psi^{gs}\rangle$ represents the ground state. $I(\omega)$ can be evaluated using the Born-Oppenheimer approximation, which makes a separation of the electronic and nuclear wave functions $|\Psi^i\rangle = |e^i\rangle|\psi^i\rangle$, and the Franck-Condon principle, whereby the heavy nuclei do not change their positions or momenta during the electronic transition. If the excited electron belongs to the impurity, the helium cluster remains frozen, so that the relevant coordinate is the relative position **r** between the cluster and the impurity. That principle amounts to assuming that D_{ge} is independent of the nuclear coordinates. Taking into account that $e^{(-it/\hbar)\mathcal{H}_{gs}}|\Psi^{gs}\rangle = e^{-it\omega_{gs}}|\Psi^{gs}\rangle$ and projecting on eigenstates of the orbital angular momentum of the excited electron $|m\rangle$,

$$I(\omega) \propto \sum_m \int dt e^{-i(\omega+\omega^{gs})t} \langle \Psi^{gs} | D_{ge}^\dagger | m \rangle e^{-(it/\hbar)\mathcal{H}_m^{ex}} \langle m | D_{ge} | \Psi^{gs} \rangle$$

$$= \sum_m \int dt e^{-i(\omega+\omega^{gs})t} \int d^3\mathbf{r} \int d^3\mathbf{r}' \langle \Psi^{gs} | \mathbf{r} \rangle$$

$$\times \langle \mathbf{r} | D_{ge}^\dagger | m \rangle e^{(it/\hbar)\mathcal{H}_m^{ex}} \langle m | D_{ge} | \mathbf{r}' \rangle \langle \mathbf{r}' | \Psi^{gs} \rangle$$

$$= |D_{ge}|^2 \sum_m \int dt e^{-i(\omega+\omega_X^{gs})t} \int d^3\mathbf{r} \psi_X^{gs}(\mathbf{r})^* e^{(it/\hbar)H_m^{ex}(\mathbf{r})} \psi_X^{gs}(\mathbf{r}), \quad (9)$$

where $\hbar\omega_X^{gs}$ and $\psi_X^{gs}(\mathbf{r})$ are the energy and the wave function of the rovibrational ground state of the frozen helium-impurity system, and $H_m^{ex}(\mathbf{r})$ is the rovibrational excited Hamiltonian with potential energy $V_m^{ex}(\mathbf{r})$ determined by the electronic energy eigenvalue, as obtained in the next subsection for a $p \leftarrow s$ transition. Equation (9) will be referred to as the *Fourier formula*, and it is the Fourier transform of the time-correlation function. It is nothing but a sum at the resonant energies weighted with the well-known Franck-Condon factors as follows:

$$I(\omega) \propto \sum_m \int dt e^{-i(\omega+\omega_X^{gs})t} \langle \psi_X^{gs} | e^{(it/\hbar)H_m^{ex}} | \psi_X^{gs} \rangle$$

$$= \sum_m \sum_{\nu\nu'} \int dt e^{-i(\omega+\omega_X^{gs})t} \langle \psi_X^{gs} | \psi_\nu^m \rangle \langle \psi_\nu^m | e^{(it/\hbar)H_m^{ex}} | \psi_{\nu'}^m \rangle$$

$$\times \langle \psi_{\nu'}^m | \psi_X^{gs} \rangle$$

$$= \sum_m \sum_\nu \int dt e^{-i(\omega+\omega_X^{gs}-\omega_\nu^m)t} |\langle \psi_\nu^m | \psi_X^{gs} \rangle|^2$$

$$= \sum_m \sum_\nu \delta(\omega+\omega_X^{gs}-\omega_\nu^m) |\langle \psi_\nu^m | \psi_X^{gs} \rangle|^2,$$

where ω_ν^m and $|\psi_\nu^m\rangle$ are the rovibrational eigenvalues and eigenstates of the Hamiltonian H_m^{ex}.

If the relevant excited states for the transition have large quantum numbers, they can be treated as approximately classical[37–39] using the averaged energy $\hbar\omega_\nu^m \approx V_m^{ex}(\mathbf{r})$ which is independent of ν. In this case we obtain the expression

$$I(\omega) \propto \sum_m \int d^3\mathbf{r} |\psi_X^{gs}(\mathbf{r})|^2 \delta(\omega+\omega_X^{gs}-V_m^{ex}(\mathbf{r})/\hbar)$$

$$= \hbar \int_{\Omega_m(\omega)} d^2\mathbf{r} \frac{|\psi_X^{gs}(\mathbf{r})|^2}{|\nabla V_m^{ex}(\mathbf{r})|}, \quad (10)$$

where $\Omega_m(\omega)$ is the surface defined by the equation $\omega+\omega_X^{gs}-V_m^{ex}(\mathbf{r})/\hbar=0$. We will refer to this equation as the *semiclassical formula*.

If the atom is in bulk liquid helium, or at the center of the drop, the problem has spherical symmetry and the above equation reduces to

$$I(\omega) \propto 4\pi \sum_m \int dr |r\psi_X^{gs}(r)|^2 \delta(\omega+\omega_X^{gs}-V_m^{ex}(r)/\hbar)$$

$$= 4\pi\hbar \sum_m \left| \frac{[r\psi_X^{gs}(r)]^2}{dV_m^{ex}(r)/dr} \right|_{r=r_m(\omega)}, \quad (11)$$

where $r_m(\omega)$ is the root of the equation $\omega+\omega_X^{gs}-V_m^{ex}(r)/\hbar=0$.

In the nonspherical case, we have evaluated $I(\omega)$ from the first expression in Eq. (10) using the discretization

$$I(n\Delta\omega + \omega_0) \propto \sum_m \sum_{ijk} |\psi_X^{gs}(\Delta\mathbf{r}_{ijk} + \mathbf{r}_0)|^2 \frac{\Delta x \Delta y \Delta z}{\Delta\omega}$$

$$\times \{\Theta[(n-1/2)\Delta\omega + \omega_0 + \omega_X^{gs}$$

$$- V_m^{ex}(\Delta\mathbf{r}_{ijk} + \mathbf{r}_0)/\hbar] - \Theta[(n+1/2)\Delta\omega + \omega_0$$

$$+ \omega_X^{gs} - V_m^{ex}(\Delta\mathbf{r}_{ijk} + \mathbf{r}_0)/\hbar]\}, \quad (12)$$

where Θ is the step function and $\Delta\omega$ is a frequency step small enough so that the above discretization represents the delta function. We also take advantage that only points near the impurity contribute to the integral, by writing $\Delta\mathbf{r}_{ijk} + \mathbf{r}_0 = (i\Delta x + x_0, j\Delta y + y_0, k\Delta z + z_0)$, with Δx, Δy, and Δz being the spatial mesh steps used in the discretization, and $\mathbf{r}_0$ an arbitrary point in the neighborhood of the impurity. Finally, we recall that $I(\omega)$ needs to be evaluated only in a narrow frequency range starting from an arbitrary ω_0 which can be, e.g., the free atom frequency. This range defines the maximum n value in the above equation.

B. Excited rovibrational potential for a $p \leftarrow s$ transition

We next determine the potential energy surfaces $V_m^{ex}(\mathbf{r})$ needed to carry out the calculation of the atomic shifts.

1. Pairwise sum approximation

The pair interaction between an atom in a s state and an atom in a p state can be expressed, in the Cartesian eigenbasis ($|x\rangle, |y\rangle, |z\rangle$), as

$$U(r) = \begin{pmatrix} V_\Pi(r) & 0 & 0 \\ 0 & V_\Pi(r) & 0 \\ 0 & 0 & V_\Sigma(r) \end{pmatrix}$$

$$= V_\Pi(r)\{|x\rangle\langle x| + |y\rangle\langle y|\} + V_\Sigma(r)|z\rangle\langle z|$$

$$= V_\Pi(r)\mathbf{I} + \{V_\Sigma(r) - V_\Pi(r)\}|z\rangle\langle z|, \quad (13)$$

where $V_\Pi(r)$ and $V_\Sigma(r)$ are the adiabatic potentials neglecting the spin-orbit interaction and r is the distance between atoms. For a system of N helium atoms and an excited impurity in a p state, the total potential is approximated by the pairwise sum

$$U = \sum_{n=1}^N \{V_\Pi(r_n)\mathbf{I} + [V_\Sigma(r_n) - V_\Pi(r_n)]R_n|z\rangle\langle z|R_n^{-1}\}, \quad (14)$$

where r_n is the distance between the nth helium atom and the impurity, and R_n is the rotation matrix that transform the unity vector $\hat{\mathbf{z}}$ into the $\hat{\mathbf{r}}_n$ vector. It can be shown that, in Cartesian coordinates,

$$\langle x^i|R_n|z\rangle\langle z|R_n^{-1}|x^j\rangle = \frac{x_n^i x_n^j}{r_n^2}, \quad (15)$$

where $x^1 = x$, $x^2 = y$, $x^3 = z$, and $r_n^2 = x_n^2 + y_n^2 + z_n^2$. Thus, the matrix elements of the total potential are

$$\langle x^i|U|x^j\rangle \equiv U_{ij} = \sum_{n=1}^N \left\{ V_\Pi(r_n)\delta_{ij} + [V_\Sigma(r_n) - V_\Pi(r_n)]\frac{x_n^i x_n^j}{r_n^2} \right\}. \quad (16)$$

Using the continuous density approach inherent to DFT $[\Sigma_n \to \int d^3\mathbf{r}'\rho(\mathbf{r}')]$, this expression can be written as

$$U_{ij}(\mathbf{r}) = \int d^3\mathbf{r}'\rho(\mathbf{r}' + \mathbf{r})\left\{ V_\Pi(r')\delta_{ij} + [V_\Sigma(r') - V_\Pi(r')]\frac{x'^i x'^j}{r'^2} \right\}. \quad (17)$$

The eigenvalues of this symmetric matrix are the sought-after $V_m^{ex}(\mathbf{r})$ which define the potential energy surfaces (PESs) as a function of the distance between the centers of mass of the droplet and of the impurity, and are given by the three real roots $\lambda_i(\mathbf{r})$ of the equation

$$\lambda^3 + C\lambda^2 + B\lambda + A = 0, \quad (18)$$

with

$$C = -\sum_{i=1}^3 U_{ii},$$

$$B = \frac{1}{2}\sum_{i\neq j}^3 (U_{ii}U_{jj} - U_{ij}^2),$$

$$A = \sum_{i\neq j\neq k}^3 \left(\frac{1}{2}U_{ii}U_{jk}^2 - \frac{1}{3}U_{ii}U_{jj}U_{kk} - \frac{2}{3}U_{ij}U_{jk}U_{ki} \right). \quad (19)$$

It can be shown that for spherical geometry, Eq. (17) is diagonal with matrix elements (in spherical coordinates)

$$\lambda_i(r) \equiv U_{ii}(r) = 2\pi \int\int r'^2 \sin\theta' d\theta' dr'$$

$$\rho(|r' + r + 2r'r\cos\theta'|)\left\{ V_\Pi(r') + [V_\Sigma(r') - V_\Pi(r')] \right.$$

$$\left. \times \left[\frac{1}{2}(\delta_{i1} + \delta_{i2})\sin^2\theta' + \delta_{i3}\cos^2\theta' \right] \right\}. \quad (20)$$

2. Spin-orbit coupling

For atomic impurities in which the spin-orbit (SO) interaction is prominent and comparable to the splitting of the P states due to the interaction with the droplet, it has to be taken into account in the calculation of the PESs. This is usually done considering that the SO splitting of the dopant is that of the isolated atom irrespective of the impurity-drop distance.[39,46,47] Given the atomic structure of alkaline earth atoms, the SO interaction can be safely neglected in the PES calculation. However, we discuss it here for the sake of completeness and future reference.

When the spin-orbit interaction is taken into account, the total potential can be written as $V_T = U + V_{SO}$, where V_{SO} has the form, in the spin-Cartesian orbit basis ($|x, 1/2\rangle$,

$$|x,-1/2\rangle, |y,1/2\rangle, |y,-1/2\rangle, |z,1/2\rangle, |z,-1/2\rangle),$$

$$V_{SO} = \frac{A_{\ell s}}{2} \begin{pmatrix} 0 & 0 & -i & 0 & 0 & 1 \\ 0 & 0 & 0 & i & -1 & 0 \\ i & 0 & 0 & 0 & 0 & -i \\ 0 & -i & 0 & 0 & -i & 0 \\ 0 & -1 & 0 & i & 0 & 0 \\ 1 & 0 & i & 0 & 0 & 0 \end{pmatrix},$$

where $A_{\ell s}$ is 2/3 of the experimental SO splitting of an isolated atom. Kramers' theorem states that there is a twofold degenerate manyfold of systems with a total half-integer spin value that cannot be broken by electrostatic interactions,[48] so that the twofold degenerate eigenvalues that define the PESs are the roots of the equation

$$\lambda^3 + C\lambda^2 + \left[B - \tfrac{3}{4}A_{\ell s}^2\right]\lambda + \left\{A + \tfrac{1}{4}[A_{\ell s}^3 - A_{\ell s}^2 C]\right\} = 0, \tag{21}$$

with A, B, and C defined in Eq. (19). In the case of spherical geometry, the eigenvalues adopt a simple expression as follows:

$$\lambda_1(r) = \tfrac{1}{2}(U_{11} + U_{33}) + \tfrac{1}{4}[-A_{\ell s} \\ + \sqrt{9A_{\ell s}^2 - 4A_{\ell s}(U_{11} - U_{33}) + 4(U_{11} - U_{33})^2}],$$

$$\lambda_2(r) = U_{11} + \frac{A_{\ell s}}{2},$$

$$\lambda_3(r) = \tfrac{1}{2}(U_{11} + U_{33}) + \tfrac{1}{4}[-A_{\ell s} \\ - \sqrt{9A_{\ell s}^2 - 4A_{\ell s}(U_{11} - U_{33}) + 4(U_{11} - U_{33})^2}], \tag{22}$$

which reduces to Eq. (20) if $A_{\ell s}=0$.

It is important to notice that for spherical geometries (spherically symmetric impurities in liquid helium or at the center of a drop), when the SO interaction is negligible two of the PESs, as it can be seen from Eq. (20), that yields $\lambda_1(r)=\lambda_2(r)\neq\lambda_3(r)$ are degenerate.[49] Thus, the existence of the SO interaction not only is the reason of the appearance of the D_1 and D_2 lines in the case, e.g., of alkali atoms in bulk liquid helium, but also the reason of either the broadening or the splitting of the D_2 line.[50] For this particular geometry, another contribution to the splitting of the D_2 line is the Jahn-Teller effect caused by dynamical quadrupole deformations of the cavity surrounding the impurity, which develop irrespective of whether the spin-orbit energy is relevant or not.[6,51] When the impurity resides in a deformed environment like a dimple, the three PESs are nondegenerate, and may cause the appearance of three distinct peaks in the absorption spectrum, or of just one single broad peak, as it happens in the case of Ca, Sr, and Ba atoms attached to ^{4}He drops.[4,5] The liquid ^{4}He results for alkaline earth atoms are reported in Refs. 52 and 53, and references therein.
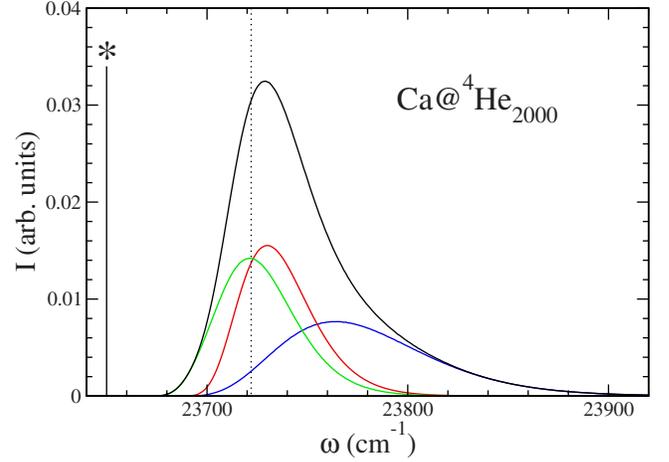

FIG. 7. (Color online) Calcium absorption spectrum for $N = 2000$ in the vicinity of the $4s4p \, ^1P_1 \leftarrow 4s^2 \, ^1S_0$ transition. The starred vertical line represents the gas-phase transition and the dotted vertical line the experimental value extracted from Fig. 3 of Ref. 4. The three components of the absorption line, each arising from a different excited PES, are also shown.

V. RESULTS FOR THE ABSORPTION SPECTRUM OF CALCIUM ATOMS

A. Line shifts

The problem of obtaining the line shifts has been thus reduced to that of the dopant in the 3D trapping potentials corresponding to the ground state, $U_{Ca}(\mathbf{r})$, and P excited states, $\lambda_i(\mathbf{r})$. Since we have neglected the fluctuations of the dimple—shape fluctuations[54]—and their coupling to the dopant dipole oscillations, as well as inhomogeneous broadening resulting from droplet size distributions, laser linewidth and similar effects, the model is not expected to yield the line shapes, but only the energies of the atomic transitions. These limitations are often overcome by introducing line shape functions or convoluting the calculated lines with some effective line profiles.[41,42] We discuss now some illustrative examples without considering these justified but somewhat uncontrolled convolutions.

Figure 7 shows the absorption spectrum of Ca@^{4}He$_{2000}$ calculated with the semiclassical formula. The much involved Fourier formula calculation is unnecessary in the Ca@^{4}He$_N$ case. The reason is the absence of bound-bound transitions from the ground state PES to the Π or Σ ones because their wells are spatially well apart. The starred vertical line represents the gas-phase transition. The three components of the absorption line, each arising from a different excited PES, are also shown. We have normalized to 1 the integral of each component. This choice comes out naturally from the normalization of the wave function of the impurity; obviously, the relative intensity of the three components is not arbitrary. In Fig. 7, the Π PESs contribute to build up the maximum of the line, whereas the long blueshift tail arises from the Σ PES.

No appreciable differences appear between $N=2000$ and 2500, the largest drop we have calculated. This saturation has been also observed in the experiment,[4,5] although for larger
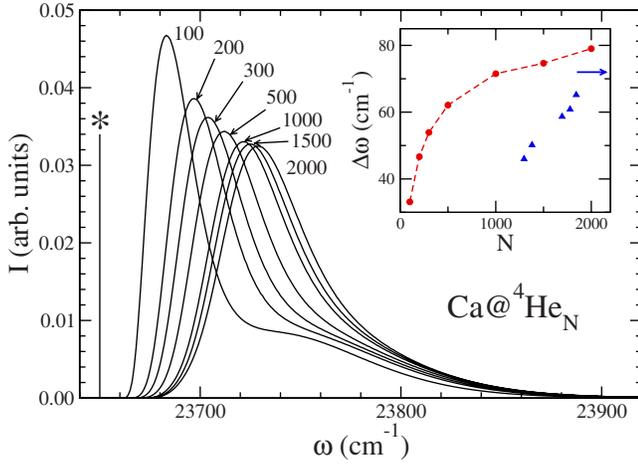
FIG. 8. (Color online) Total absorption spectrum of Ca attached to $^4\text{He}_N$ droplets in the vicinity of the $4s4p\ ^1P_1 \leftarrow 4s^2\ ^1S_0$ transition, for the indicated N values. The starred vertical line represents the gas-phase transition. The inset shows the calculated shifts relative to the gas-phase transition (dots), defined as the energy of the maximum of the absorption line minus the energy of the gas-phase transition. The experimental values are also shown (triangles). The arrow indicates the asymptotic experimental value (Ref. 4).

mean cluster sizes, about $N \sim 3000$. The peak energy is 79 cm^{-1}, 10% larger than the experimental saturation value of 72 cm^{-1},[4] which indicates a fairly good agreement between theory and experiment. The calculated width [full width at half maximum (FWHM)] is ~ 55 cm^{-1}, whereas the measured width for drops in the $N = 1500$–2000 range is ~ 140–155 cm^{-1},[4] i.e., about three times larger. We will show later how thermal motion affects the theoretical result.

Figure 8 shows the total absorption spectrum of Ca attached to $^4\text{He}_N$ droplets for several N values. It is interesting to notice the evolution of the absorption line as the number of atoms increases. As a general rule, the smaller the drop, the smaller the splitting of the Π components. Indeed, they would be degenerate if $N = 1$, as Eq. (13) shows. This explains why the main peak for $N = 100$ is the narrower one, and is the reason why the main peak is fairly apart from the Σ shoulder. As N increases, so it does the splitting, while the three components of the peak become broader. Eventually, if N is large enough, it is not possible to distinguish the components of the absorption line. It is also obvious that line broadening due to effects not considered here may wash out the blueshifted shoulder found for small N values.

The inset in Fig. 8 shows the calculated shifts relative to the gas-phase transition, compared with the experimental values.[4] One can appreciate a small oscillation for the largest drops; it is a genuine effect produced by the dimple structure. Further insight can be gained from the study of the absorption spectrum as a function of $\mathcal{Z}_0$. To this end, we display in the top panel of Fig. 9 the absorption spectra for the $N = 500$ droplet corresponding to $\mathcal{Z}_0$ values from 16 to 19 Å in 0.5 Å steps, all of them within the drop surface region (the equilibrium value is $\mathcal{Z}_0 = 17.45$ Å). The inset in Fig. 9 shows the dependence of the relative shift on the location of the Ca atom. One can see how a 3 Å dispersion in the position of the impurity generates an ~ 45 cm^{-1} change in the shift,
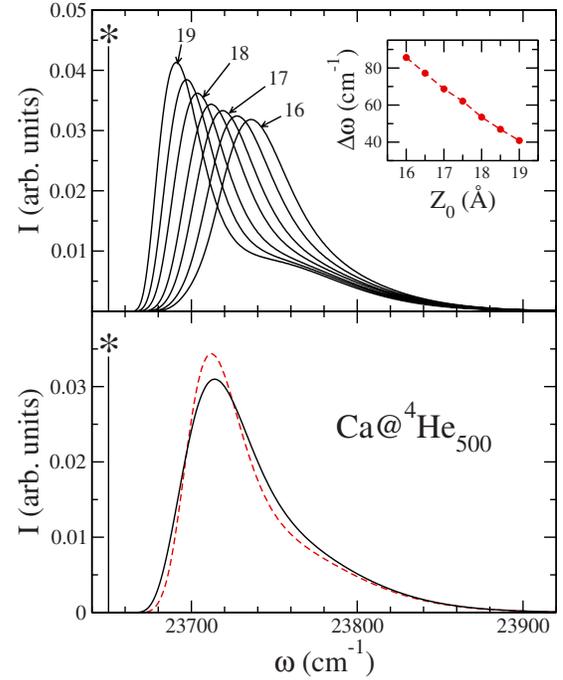

FIG. 9. (Color online) Bottom panel: Thermally averaged absorption spectrum of Ca in a $N = 500$ drop (solid line); the dashed line represents the absorption spectrum corresponding to the equilibrium configuration. Top panel: $I_i(\omega)$ spectra used to carry out the average. The $\mathcal{Z}_{0_i}$ values go from 16 to 19 Å in 0.5 Å steps. The inset shows the associated atomic shifts.

showing in a quantitative way the well-known sensitivity of this quantity to the structure and depth of the dimple. It is worth seeing how the shift decreases as the distance between the centers of mass increases, and at the same time the absorption peak becomes more asymmetric as the Ca environment does (see also Sec. V C).

B. Thermal broadening

As we have indicated, for very attractive impurities, the foreign atom is fully solvated, and its delocalization in the bulk of the drop due to thermal motion hardly introduces a significant change in the line shape. When the dopant is in a dimple state, it has to be checked whether thermal motion may have observable effects on the absorption spectrum, as Fig. 6 seems to indicate for calcium.

To ascertain this effect, we have carried out a thermal average of the spectrum using an approximate expression for the probability density. Referring the energy E_i of a given $\mathcal{Z}_{0_i}$ configuration to the equilibrium value, $\Delta E_i = E_i - E_{\text{gs}}$, and neglecting the kinetic energy of the impurity and the displaced fluid, we write the probability density for the position $\mathcal{Z}_{0_i}$ of the Ca atom as

$$w_i = \frac{\mathcal{Z}_{0_i}^2 e^{-\Delta E_i/k_B T}}{\sum_j \mathcal{Z}_{0_j}^2 e^{-\Delta E_j/k_B T} \Delta \mathcal{Z}_{0_j}}, \tag{23}$$

where k_B is the Boltzmann constant, $T = 0.4$ K, and the sum—actually integral—runs on the selected $\mathcal{Z}_{0_i}$

configurations.[55] The $\mathcal{Z}_{0_i}^2$ factor takes care of the relative volume available to each configuration. With this definition the probability of finding the Ca atom between $\mathcal{Z}_{0_i}$ and $\mathcal{Z}_{0_i} + \Delta\mathcal{Z}_{0_i}$ is $w_i \Delta\mathcal{Z}_{0_i}$. We show in the top panel of Fig. 6 the probability densities w_i corresponding to the configurations displayed in the bottom panel. We see that there is a non-negligible probability of finding the Ca atom in a broad region of the drop surface, and consequently we have addressed, as a case of study, the statistical properties of the Ca@^{4}He$_{500}$ system at this temperature.

We have found that the mean position, calculated as $\langle\mathcal{Z}_0\rangle = \Sigma_i \mathcal{Z}_{0_i} w_i \Delta\mathcal{Z}_{0_i}$, and the standard deviation, calculated as $\sigma(\mathcal{Z}_0) = \sqrt{\langle\mathcal{Z}_0^2\rangle - \langle\mathcal{Z}_0\rangle^2}$, are 17.38 and 0.76 Å, respectively. This dispersion in the position generates a dispersion in the value of the shift. To quantify this effect we have evaluated the mean value of the shift, calculated as $\langle\Delta\omega\rangle = \Sigma_i \Delta\omega_i w_i \Delta\mathcal{Z}_{0_i}$, and its standard deviation, calculated as $\sigma(\Delta\omega) = \sqrt{\langle\Delta\omega^2\rangle - \langle\Delta\omega\rangle^2}$, using the values shown in the inset of the top panel of Fig. 9, which correspond to the seven lower energy configurations in Fig. 6. We have obtained $\langle\Delta\omega\rangle \pm \sigma(\Delta\omega) = 63.8 \pm 11.5$ cm^{-1}.

The thermally averaged Ca absorption spectrum is shown in the bottom panel of Fig. 9 (solid line), as well as that corresponding to the equilibrium configuration (dashed line). To carry out the average, we have used the $I_i(\omega)$ in the top panel of Fig. 9, and averaged them as $I(\omega) = \Sigma_i I_i(\omega) w_i \Delta\mathcal{Z}_{0_i}$. This procedure, consistent with the Franck-Condon principle, assumes that absorption proceeds instantaneously on any of the frozen drop-Ca configurations characterized by a $\mathcal{Z}_{0_i}$ value.

We are led to conclude that the thermal motion effect is rather small. It increases the FWHM by about 10%, from $\sim$49.5 to $\sim$55.0 cm^{-1}, still a factor of 3 smaller than the experimental value. From Fig. 6, we expect a similar effect for the $N=1000$ drop, and likely for larger drops.

C. Calcium atoms attached to vortex lines in ^{4}He drops

Since ^{4}He is a superfluid, it is quite natural to wonder about the appearance and detection of quantized vortices in droplets, see, e.g., Refs. 3 and 57, and references therein. Adapting an idea originally put forward by Close et al.,[58] it has been proposed[10] that Ca atoms should be the dopant of choice to detect vortices by means of microwave spectroscopy experiments. The rationale of this proposal is that Ca atoms are barely stable on the drop surface and become solvated in its interior in the presence of a vortex line.[10] These conclusions were drawn from DFT calculations using Meyer's Ca-He potential which, as shown in Fig. 1, is slightly more attractive than recent potentials. If this scenario were plausible, one would not need the microwave spectroscopy experiments suggested in Ref. 10 to detect a vortex state in a Ca@^{4}He$_N$ drop: LIF spectroscopy could do the job, given the sizable difference between the blueshifts of the absorption lines when Ca has been drawn inside the drop by the vortex (similar in value to the liquid helium blueshift), and when it resides in a dimple state in vortex-free drops.[4]
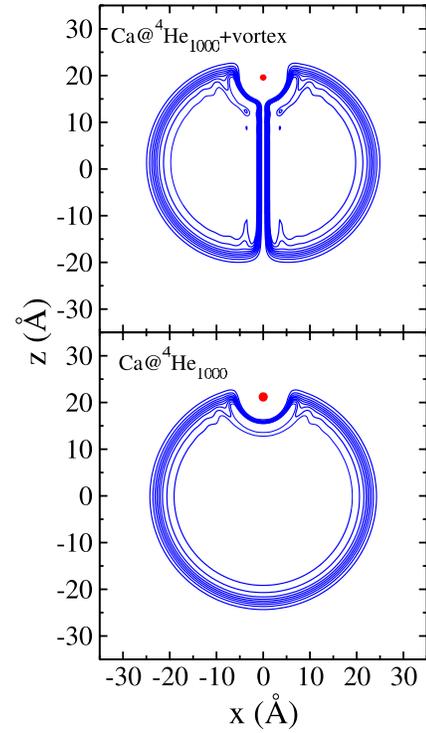

FIG. 10. (Color online) Equidensity lines showing the equilibrium configuration of a Ca atom on a ^{4}He$_{1000}$ droplet with a vortex line along its symmetry axis (top panel), and without it (bottom panel). The lines correspond to densities $0.9\rho_0$ to $0.1\rho_0$ in $0.1\rho_0$ steps; these lines span the drop surface region as well as the vortex core. The equidensity lines of the Ca probability density are similarly plotted starting from its maximum value.

This has prompted us to reanalyze the structure of a large $N=1000$ drop hosting a calcium atom attached to a vortex line along the symmetry axis. Within DFT, a robust method to generate vortex configurations in liquid helium is described in Ref. 59. We adapt it here to the case of helium drops. For a $n=1$ quantum circulation vortex line, we start the imaginary time evolution to solve Eq. (2) from the initial state

$$\Psi(\mathbf{r}) = \frac{\rho^{1/2}(\mathbf{r})}{\sqrt{x^2 + y^2}}(x + \iota y) \qquad (24)$$

if x and y are nonvanishing, and zero otherwise, where $\rho(\mathbf{r})$ is the vortex-free Ca@^{4}He$_{1000}$ helium density. After the minimization procedure is converged, we have checked that the obtained final configuration is indeed a $n=1$ vortex state.

Figure 10 shows equidensity lines for the equilibrium configuration of Ca@^{4}He$_{1000}$ with and without a vortex line along its symmetry axis. It can be seen that the vortex line draws the impurity toward the bulk of the droplet, but it still resides in a deeper surface dimple.

Figure 11 shows the absorption spectrum for the two configurations displayed in Fig. 10. The effect of the presence of the vortex on the absorption spectrum of calcium is twofold. On the one hand, the maximum of the absorption peak is shifted toward the bulk value because of the deeper dimple. On the other hand, the FWHM increases by about a factor of
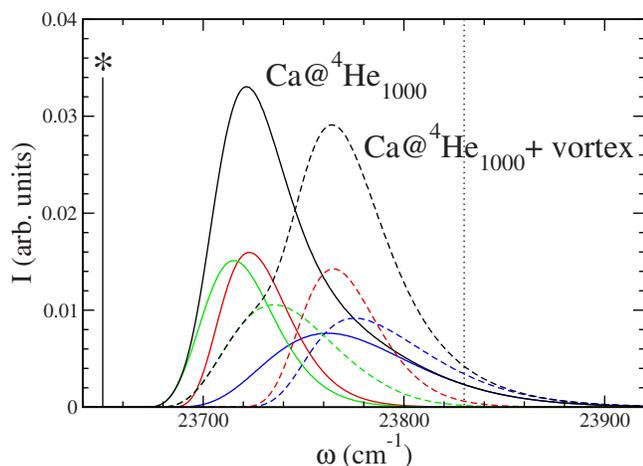
FIG. 11. (Color online) Ca absorption spectrum for the N =1000 droplet of Fig. 10 with (dashed lines) and without a vortex line along its symmetry axis (solid lines). The absorption line has been decomposed into its three components. The starred vertical line represents the gas-phase transition and the dotted vertical line represents the experimental value for bulk liquid ^{4}He (Ref. 11).

2. The reason is the spreading of the Ca wave function within the stretched $U_{Ca}(\mathbf{r})$ well, which allows the atom to "probe" a wider region in the excited PES, thus increasing the width. Notice also the larger splitting of the peaks that form the line due to the more anisotropic helium environment. This also contributes to increasing the width of the absorption peak. Unfortunately, the experimental absorption line is so broad and asymmetric that the extra shift caused by the vortex is not enough to displace the line to a region where it could be distinguishable on top of the vortex-free absorption line.

VI. SUMMARY

Within density functional theory, we have carried out a detailed study of the absorption spectrum of calcium atoms attached to ^{4}He$_N$ drops in the vicinity of the $4s4p$ $^1P_1$ $\leftarrow 4s^2$ $^1S_0$ transition, finding a semiquantitative agreement with experiment. To this end, we have improved our previous implementation of the DFT method by incorporating the zero point motion of the impurity, and have carried out *ab initio* calculations to obtain the excited $^1\Sigma$ and $^1\Pi$ Ca-He potentials needed to obtain the potential energy surfaces.

We have studied the drop structure, finding that the "interference" between the density oscillations of the helium moiety arising from its intrinsic structure and those arising from the presence of the impurity plays a role in the determination of the position of the impurity. This may be relevant for the solvation of alkaline earth atoms, especially for magnesium.[35]

In a case of study, we have systematically addressed the dependence of the relative shift on the position of the impurity, quantitatively assessing the relevance of a proper description of the dimple to reproduce the experimental results. We have statistically taken into account the influence of the thermal motion of the impurity on the absorption line, concluding that it only increases the linewidth by a modest amount.

Finally, we have addressed the Ca absorption spectrum when the helium drop hosts a vortex line, and conclude that absorption spectroscopy experiments on these drops would be likely unable to ascertain the presence of vortical states. In spite of this, the study of vortex lines pinned by calcium atoms in superfluid helium drops is interesting by itself, especially the evaluation of the atomic shift caused by the presence of a vortex line.

[1] F. Stienkemeier and A. F. Vilesov, J. Chem. Phys. **115**, 10119 (2001).
[2] F. Stienkemeier and K. K. Lehmann, J. Phys. B **39**, R127 (2006).
[3] M. Barranco, R. Guardiola, S. Hernández, R. Mayol, and M. Pi, J. Low Temp. Phys. **142**, 1 (2006).
[4] F. Stienkemeier, F. Meier, and H. O. Lutz, J. Chem. Phys. **107**, 10816 (1997).
[5] F. Stienkemeier, F. Meier, and H. O. Lutz, Eur. Phys. J. D **9**, 313 (1999).
[6] J. Reho, U. Merker, M. R. Radcliff, K. K. Lehmann, and G. Scoles, J. Chem. Phys. **112**, 8409 (2000).
[7] A. Przystawik, S. Göde, J. Tiggesbäumker, and K.-H. Meiwes-Broer, Contribution to the XXII International Symposium on Molecular Beams, University of Freiburg, 2007 (unpublished).
[8] A. Hernando, R. Mayol, M. Pi, M. Barranco, F. Ancilotto, O.

Bünermann, and F. Stienkemeier, J. Phys. Chem. A **111**, 7303 (2007).
[9] Y. Ren and V. V. Kresin, Phys. Rev. A **76**, 043204 (2007).
[10] F. Ancilotto, M. Barranco, and M. Pi, Phys. Rev. Lett. **91**, 105302 (2003).
[11] Y. Moriwaki and N. Morita, Eur. Phys. J. D **33**, 323 (2005).
[12] E. Czuchaj, F. Rebentrost, H. Stoll, and H. Preuss, Chem. Phys. Lett. **182**, 191 (1991).
[13] H. Partridge, J. R. Stallcop, and E. Levin, J. Chem. Phys. **115**, 6471 (2001).
[14] R. J. Hinde, J. Phys. B **36**, 3119 (2003).
[15] C. C. Lovallo and M. Klobukowski, J. Chem. Phys. **120**, 246 (2004).
[16] W. Meyer (private communication).
[17] E. Czuchaj, M. Krośnicki, and H. Stoll, Chem. Phys. **292**, 101

(2003).

[18] H.-J. Werner and P. J. Knowles, J. Chem. Phys. **82**, 5053 (1985).

[19] P. J. Knowles and H.-J. Werner, Chem. Phys. Lett. **115**, 259 (1985).

[20] H.-J. Werner and P. J. Knowles, J. Chem. Phys. **89**, 5803 (1988).

[21] P. J. Knowles and H.-J. Werner, Chem. Phys. Lett. **145**, 514 (1988).

[22] J. Koput and K. A. Peterson, J. Phys. Chem. A **106**, 9595 (2002).

[23] D. E. Woon and T. H. Dunning, Jr., J. Chem. Phys. **100**, 2975 (1994).

[24] H.-J. Werner, P. J. Knowles, R. Lindh, M. Schütz, P. Celani, T. Korona, F. R. Manby, G. Rauhut, R. D. Amos, A. Bernhardsson, A. Berning, D. L. Cooper, M. J. O. Deegan, A. J. Dobbyn, F. Eckert, C. Hampel, G. Hetzer, A. W. Lloyd, S. J. McNicholas, W. Meyer, M. E. Mura, A. Nicklass, P. Palmieri, R. Pitzer, U. Schumann, H. Stoll, A. J. Stone, R. Tarroni, and T. Thorsteinsson, MOLPRO version 2002.6, a package of *ab initio* programs, 2003; see http://www.molpro.net

[25] F. Dalfovo, A. Lastri, L. Pricaupenko, S. Stringari, and J. Treiner, Phys. Rev. B **52**, 1193 (1995).

[26] L. Giacomazzi, F. Toigo, and F. Ancilotto, Phys. Rev. B **67**, 104501 (2003).

[27] L. Lehtovaara, T. Kiljunen, and J. Eloranta, J. Comput. Phys. **194**, 78 (2004).

[28] F. Ancilotto, M. Barranco, F. Caupin, R. Mayol, and M. Pi, Phys. Rev. B **72**, 214522 (2005); F. Ancilotto, M. Pi, R. Mayol, M. Barranco, and K. K. Lehmann, J. Phys. Chem. A **111**, 12695 (2007).

[29] M. Frigo and S. G. Johnson, Proc. IEEE **93**, 216 (2005).

[30] W. H. Press, S. A. Teulosky, W. T. Vetterling, and B. P. Flannery, *Numerical Recipes in Fortran 77: The Art of Scientific Computing* (Cambridge University Press, Cambridge, 1999).

[31] F. Ancilotto, D. G. Austing, M. Barranco, R. Mayol, K. Muraki, M. Pi, S. Sasaki, and S. Tarucha, Phys. Rev. B **67**, 205311 (2003).

[32] S. A. Chin and E. Krotscheck, Phys. Rev. B **45**, 852 (1992).

[33] A. Hernando, F. Ancilotto, M. Barranco, R. Mayol, and M. Pi (unpublished).

[34] J. P. Toennies and A. F. Vilesov, Angew. Chem., Int. Ed. **43**, 2622 (2004).

[35] M. Mella, G. Calderoni, and F. Cargnoni, J. Chem. Phys. **123**, 054328 (2005).

[36] M. Elhiyani and M. Lewerenz, Contribution to the XXII International Symposium on Molecular Beams, University of Freiburg, 2007 (unpublished).

[37] M. Lax, J. Chem. Phys. **20**, 1752 (1952).

[38] E. Cheng and K. B. Whaley, J. Chem. Phys. **104**, 3155 (1996).

[39] A. Nakayama and K. Yamashita, J. Chem. Phys. **114**, 780 (2001).

[40] M. Mella, M. C. Colombo, and F. G. Morosi, J. Chem. Phys. **117**, 9695 (2002).

[41] F. Stienkemeier, J. Higgins, C. Callegari, S. I. Kanorsky, W. E. Ernst, and G. Scoles, Z. Phys. D: At., Mol. Clusters **38**, 253 (1996).

[42] O. Bünermann, G. Droppelmann, A. Hernando, R. Mayol, and F. Stienkemeier, J. Phys. Chem. A **111**, 12684 (2007).

[43] F. O. Ellison, J. Am. Chem. Soc. **85**, 3540 (1963).

[44] The vibrational frequency of the Ca atom in the potential of Eq. (4) can be estimated taking it as approximately harmonic in view of the Gaussian-like shape of the ground state wave function, see Fig. 5. For $N=2000$, we get $\hbar\omega=2[\varepsilon-U_{Ca}(\mathbf{r}_{min})]/3\sim 2[-57.4-(-67.2)]/3=6.5$ K.

[45] K. K. Lehmann and A. M. Dokter, Phys. Rev. Lett. **92**, 173401 (2004).

[46] J. S. Cohen and B. Schneider, J. Chem. Phys. **61**, 3230 (1974).

[47] Z. J. Jakubek and M. Takami, Chem. Phys. Lett. **265**, 653 (1997).

[48] P. H. E. Meier and E. Bauer, *Group Theory* (North-Holland, Amsterdam, 1962).

[49] This statement holds for $r\neq 0$, and it is relevant when we take into account the delocalization of the impurity inside the bubble due to the zero point motion. Otherwise, since at $r=0$ all the λ_i coincide (as they should), the degeneracy would be 3.

[50] T. Kinoshita, K. Fukuda, Y. Takahashi, and T. Yabuzaki, Phys. Rev. A **52**, 2707 (1995).

[51] T. Kinoshita, K. Fukuda, and T. Yabuzaki, Phys. Rev. B **54**, 6600 (1996).

[52] H. Bauer, M. Beau, B. Friedl, C. Marchand, and K. Miltner, Phys. Lett. A **146**, 134 (1990).

[53] Y. Moriwaki, K. Inui, K. Kobayashi, F. Matsushima, and N. Morita, J. Mol. Struct. **786**, 112 (2006).

[54] P. B. Lerner, M. B. Chadwick, and I. M. Sokolov, J. Low Temp. Phys. **90**, 319 (1993).

[55] It is worth recalling that the effective mass m^* of the Ca atom will depend on $\mathcal{Z}_0$ since the volume of the displaced liquid depends on the size of the dimple. We can obtain a lower bound for m^* as the mass of the free Ca atom, 40 a.u., and an upper bound as the hydrodynamic mass of Ca in bulk helium (Ref. 56), 64 a.u. In the harmonic approximation, we can estimate the quantum of energy as $\hbar\omega=\sqrt{\hbar^2 E''(\mathcal{Z}_0)|_{min}/m^*}$, finding for each bound a value around 0.3 and 0.25 K, respectively. In the same approximation, the population at $T=0.4$ K of the excited states p_{ex} relative to that of the ground state p_0, calculated as $p_{ex}/p_0 =\Sigma_{n=1}^{\infty}\exp(-n\hbar\omega/k_B T)$, is $\sim$0.3 and 0.4, respectively. These values are large enough to justify the semiclassical approximation for the average on the initial states, namely, $\Sigma_n \exp(-\Delta E_n/ k_B T)\rightarrow 4\pi\int d\mathcal{Z}_0\mathcal{Z}_0^2 \exp[-\Delta E(\mathcal{Z}_0)/k_B T]$.

[56] K. K. Lehmann, Phys. Rev. Lett. **88**, 145301 (2002).

[57] K. K. Lehmann and R. Schmied, Phys. Rev. B **68**, 224520 (2003).

[58] J. D. Close, F. Federman, K. Hoffmann, and N. Quaas, J. Low Temp. Phys. **111**, 661 (1998).

[59] M. Pi, R. Mayol, A. Hernando, M. Barranco, and F. Ancilotto, J. Chem. Phys. **126**, 244502 (2007).